Multicolor Fluorescence Nanoscopy by Photobleaching: Concept, Verification, and Its Application To Resolve Selective Storage of Proteins in Platelets

Daniel Rönnlund,[†,*] Lei Xu,[†] Anna Perols,[‡] Annica K. B. Gad,[§] Amelie Eriksson Karlström,[‡] Gert Auer,[∥] and Jerker Widengren[†,*]

[†]Department of Applied Physics, Royal Institute of Technology, Stockholm, 106 91 Sweden, [‡]Department of Molecular Biotechnology, Royal Institute of Technology, Stockholm, 106 91 Sweden, [§]Department of Microbiology, Tumor and Cell Biology, Karolinska Institutet, Stockholm, 171 77 Sweden, and [∥]Department of Oncology and Pathology, Karolinska Institute, Stockholm, 171 77 Sweden

ABSTRACT Fluorescence nanoscopy provides means to discern the finer details of protein localization and interaction in cells by offering an order of magnitude higher resolution than conventional optical imaging techniques. However, these super resolution techniques put higher demands on the optical system and the fluorescent probes, making multicolor fluorescence nanoscopy a challenging task. Here we present a new and simple procedure, which exploits the photostability and excitation spectra of dyes to increase the number of simultaneous recordable targets in STED nanoscopy. We use this procedure to demonstrate four-color STED imaging of platelets with ≤40 nm resolution and low crosstalk. Platelets can selectively store, sequester, and release a multitude of different proteins, in a manner specific for different physiological and disease states. By applying multicolor nanoscopy to study platelets, we can achieve spatial mapping of the protein organization with a high resolution for multiple proteins at the same time and in the same cell. This provides a means to identify specific platelet activation states for diagnostic purposes and to understand the underlying protein storage and release mechanisms. We studied the organization of the pro- and antiangiogenic proteins VEGF and PF-4, together with fibrinogen and filamentous actin, and found distinct features in their respective protein localization. Further, colocalization analysis revealed only minor overlap between the proteins VEGF and PF-4 indicating that they have separate storage and release mechanisms, corresponding well with their opposite roles as pro- and antiangiogenic proteins, respectively.

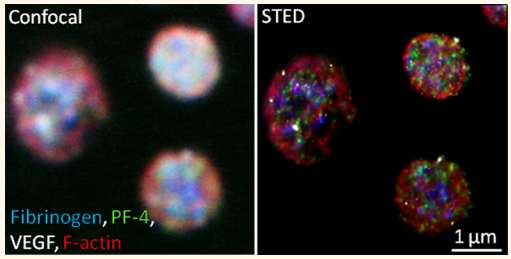

KEYWORDS: multicolor · super resolution microscopy · photobleaching · STED · platelets · thrombocytes · α-granules

Fluorescence microscopy is an important tool in molecular and cellular biology. A wide range of synthetic dyes and fluorescent proteins with different emission spectra and lifetimes make it possible to simultaneously detect and separately analyze multiple molecular targets. Usually, the labeling targets are proteins of only a few nanometers in size. The fine details of protein storage and interaction can therefore not be fully resolved in conventional optical imaging techniques such as wide-field or confocal microscopy, where the resolution is limited to a few hundreds of nanometers.[1] Recent developments in fluorescence nanoscopy, with techniques such as STED,[2,3] PALM,[4] and STORM[5] offering an order of magnitude higher resolution, now drastically improve the means of overcoming these limitations. However, these super resolution techniques put higher and more specific demands on the optical system as well as on the fluorescent probes. As a consequence, fluorescent nanoscopy images with more than two colors are hard to acquire outside the leading specialized laboratories.[6,7]

The principle of STED microscopy is very similar to that of confocal microscopy, with the addition of a second laser beam featuring a central intensity zero in its focus (commonly shaped as a doughnut). By inducing stimulated emission, this second beam acts to "turn off" all excited molecules which lie outside of the very center of the focus. This effectively shrinks the excitation

* Address correspondence to danron@kth.se, jwideng@kth.se.

Received for review November 27, 2013 and accepted April 14, 2014.

Published online April 14, 2014
10.1021/nn406113m

volume and thereby increases the resolution directly during image capture, without the need of any computations. For additional information, we refer to good review articles.[8,9]

Localization based fluorescence nanoscopy techniques such as PALM and STORM are based on the sequential on/off switching and individual localization of fluorescent probes. If only single probes are active inside the diffraction volume, their position can be computationally localized with very high precision.[10] By stochastically switching on a small subset of the fluorescent probes in each image, localizing their individual positions, and then repeating this procedure, we can obtain a high resolution image from the combined localizations. Using this principle, Zhuang and co-workers recently reported a 4-color STORM image on cells[6] and a 6-color STORM image on a model sample.[11] However, due to the very different procedure involved in the acquisition of the high resolution image and in the labeling of the target molecules, the multicolor procedure cannot be directly applied to STED imaging. Since both STED and PALM/STORM have their selective advantages, it is of interest to establish multicolor acquisition possibilities for both categories of super resolution imaging techniques.

For STED and conventional fluorescence microscopy, the most common way to perform multicolor fluorescence imaging is to label targets with fluorescent probes having different excitation and emission spectra, requiring different excitation lasers as well as fluorescence emission pathways for each target. However, the addition of the extra beam in STED imaging makes spectral separation of more than two dyes challenging. Another option is to add the fluorescent lifetime as a read out parameter, whereby dyes with short and long lifetimes can be separated.[12] However, this requires high time resolution and also high emission intensity to reduce crosstalk between the targets. Using fluorescence lifetime to separate dyes can therefore be challenging in STED nanoscopy where the emission intensity is generally lower due to less fluorescent probes being active at the same time. Nonetheless, successful STED imaging has been achieved in combination with lifetime separation with <10% crosstalk.[7] Here we demonstrate how the excitation spectrum and photostability of the dyes can be exploited to add the possibility of imaging additional targets with little or no modification of the microscope setup needed. We use this method to demonstrate four-color STED imaging of platelets with low crosstalk at $\leq$40 nm resolution.

Platelets act as the postal office of our body. While circulating the bloodstream, they are capable to selectively store, sequester, and release a large number of different molecules and proteins.[13] Due to their highly sensitive nature, platelets can be activated by many different molecules resulting in morphological changes followed by release or uptake of specific proteins.[14−18] Thereby platelets can release certain proteins where they are needed, such as fibrinogen at the location of a wound[19] or growth proteins such as VEGF at the location of rapid cell division.[20] Details of how proteins are stored in platelets thus carry a wealth of information regarding the status of our bodies and can potentially provide diagnostic indicators of different states and diseases, including cancer.[21,22] Further, the mechanisms behind the selective protein uptake and release in platelets are still under debate.[23,24] Improved means for characterization of proteins in intact platelets will not only sharpen the diagnostics but also provide a deeper understanding of these underlying mechanisms which could provide a basis for various treatment regimes. To extract the necessary information it is beneficial to be able to label and specifically detect multiple targets simultaneously. In addition, platelets are typically small, in the order of 2−4 μm^2, and recent studies indicate that the carried proteins are stored in separate compartments inside 200−500 nm α-granules.[24−26] High resolution is therefore needed to elucidate this fine compartmentalization, making multicolor STED nanoscopy an ideal tool to further exploit the diagnostic and therapeutic potential of platelet proteomics.

RESULTS AND DISCUSSION

Given the central role of platelets in early cancer development, in particular their ability to selectively store and release proteins regulating tumor development, it is of considerable benefit to be able to simultaneously localize multiple proteins with high resolution and specificity within individual, intact platelets. This provides a motivation to develop further means to monitor multiple targets with super resolution STED imaging. In the following, we describe the developed procedures and their application to multiple target high resolution imaging on intact platelets.

Overall Strategy for Multicolor Acquisition. In the procedure, two targets (referred to as A and B) are labeled with fluorescent molecules which have similar emission and excitation profiles but different photostability. An image is acquired using a single excitation and emission pathway resulting in a combined image of the two targets (A + B), as shown in Figure 1a. Thereafter, a laser is used to photobleach one of the targets (A), while the other target (B) remains largely unaffected. A new image is then acquired, now only showing the unaffected target (B). By removing the image of the unaffected target (B) from that of the combined targets (A + B), we can extract an image of the bleached target as A = (A + B) − B. Further, if the microscope already has the possibility to distinguish between two different targets by separate excitation and emission pathways, this method can be applied in both channels to produce a four-color image as shown in Figure 1b. In principle, the method could also be used together with other means of separating targets, for instance by

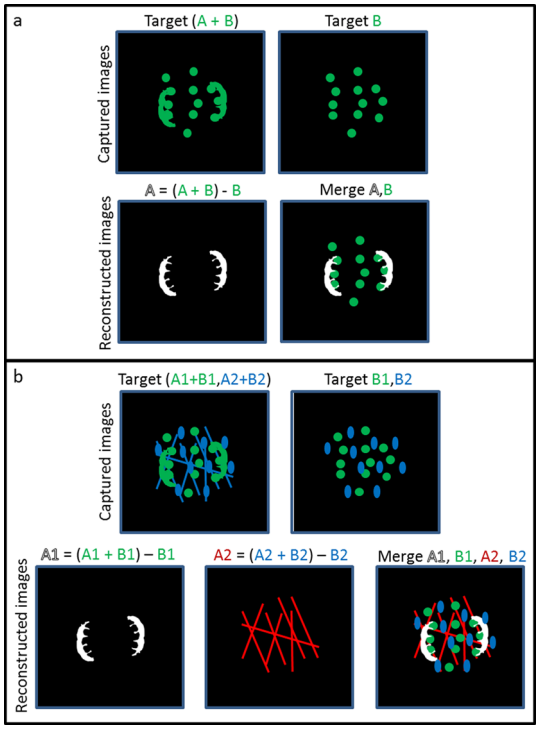

Figure 1. Schematic display of the imaging procedure. (a) Two images are captured, the first showing both targets (A + B) and the second showing the stable target (B) where target (A) has been bleached. The image of (A) can be reconstructed by subtracting the second image from the first as A = (A + B) − B. Finally, a merged image can be made where both targets are separated (A, B). (b) If the microscope can perform dual channel imaging by some means (for instance, by use of emission wavelength or fluorescence lifetime separation), the method can be applied to create an image separating four different targets. The first captured image shows the combined image of all four targets (A1 + B1, A2 + B2) registered in the two channels and the second only the stable dyes (B1, B2). The images of the bleached dyes (A1) and (A2) can be reconstructed by the two captured images and a merge of all four targets can then be made (A1, B1, A2, B2).

fluorescence lifetime, thereby increasing the number of possible targets by an additional factor of 2.

The requirement is that we can, to a large extent, bleach one of the targets while keeping the other unaffected. For this to work it is of benefit if there is a slight difference between the excitation spectra of the two dyes. Even a difference of just a few nanometers can give a substantial difference in the excitation rate if the laser wavelength is selected at the long wavelength end tail of the excitation spectra. We used antibodies coupled to the fluorophores Atto647N and Dylight650 where in water solution we measured a ∼8 nm shift toward longer wavelengths in the excitation spectrum of Dylight650, as shown in Figure S1a. We chose to bleach at a wavelength of 710 ± 10 nm where Dylight650 had an approximately 3−4 times higher excitation cross section as compared to Atto647N. For the second channel, we could use the same dye Alexa594 coupled to either antibodies or phalloidin. Here we noticed a large change in photostability depending on the conjugation together with a slight shift in the excitation spectrum, with the spectrum of Alexa594-phalloidin shifted ∼2 nm toward longer wavelengths as compared to Alexa594-ab. Most likely, this spectral change is too small to yield a significant difference in the excitation rate at the selected bleaching wavelength of 647 ± 5 nm, (Figure S1b). The observed dye conjugation dependent difference in the bleaching rate of Alexa594 is probably rather related to a change in the photobleaching quantum yield.

The selected bleaching wavelengths were chosen to fit the laser lines already available on our microscope, where 647 ± 5 nm is used to excite Atto647N and Dylight650 and 710 ± 10 nm is used for STED of Alexa594. Thus, applying the method did not require any changes of the optical setup (see Methods, STED Microscopy for details). However, adding one or two bleaching lasers to an optical setup is generally not difficult since properties such as beam quality and focusing is of less importance as long as the laser has sufficient power to bleach the dyes. Since we use the STED wavelength of Alexa594 to bleach Dylight650, we needed to separately take the STED image of Dylight650 combined with Atto647N before we took the STED image of Alexa594. Therefore, to acquire a four-channel image, we needed to acquire three images in total. First, the combination of Dylight650 and Atto647N (A1 + B1) was imaged, then Atto647N together with Alexa594-phalloidin and Alexa594-ab (B1, A2 + B2) where Dylight650 (A1) was bleached by the 710 ± 10 nm STED beam during capture. After the second image, a bleaching step was performed using the 647 ± 5 nm beam to remove Alexa594-phalloidin, and then the third and last image was acquired showing only Alexa594-ab (B2). When all three images are acquired, the images of the bleached dyes Alexa594-phalloidin and Dylight650-ab can be reconstructed and a merge of all four channels can be created as shown in Figure 2. Images of structured cytoskeletal targets including filamentous actin, microtubules, and vimentin intermediate filaments using the same procedure can be found in Figure S2.

Crosstalk. In general, when capturing multicolor images of different targets, the crosstalk, *i.e.*, the fraction of signal of a fluorescent molecule assigned to the wrong color channel, needs to be taken into account. In our approach, crosstalk comes from three separate sources. The first is the fraction of remaining intensity of the bleachable dye, the second the fraction of bleached intensity of the stable dye and the third is due to noise. The remaining intensity of the bleachable dye will lead to crosstalk to the image of the stable dye, while the bleached intensity of the stable dye will lead to crosstalk to the image of the bleachable dye, as shown in Figure S3. To obtain information regarding the bleached intensities of the dyes, control samples for each target need to be separately prepared and then imaged using the same labeling and imaging conditions as for the multicolor samples. This will provide knowledge

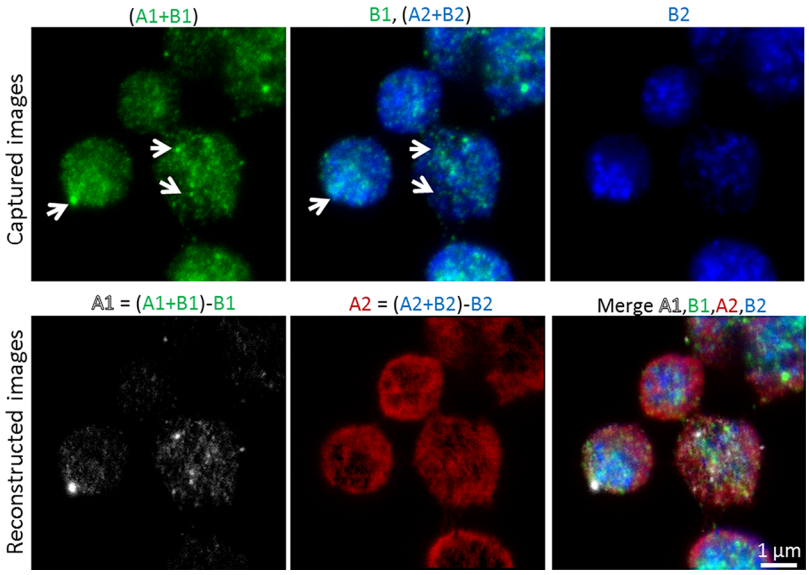

Figure 2. Captured and reconstructed images of platelets. Three images were captured where the first shows Dylight650-ab and ATTO647N-ab (A1 + B1); the second ATTO647N-ab, Alexa594-phalloidin and Alexa594-ab (B1, A2 + B2); and the third only Alexa594-ab (B2). The arrows mark some regions which were clearly bleached between the first and second image, indicating Dylight650 labeling. The images of Dylight650-ab (A1) and Alexa594-phalloidin (A2) can be reconstructed, and a merge of all STED images can be created (A1, B1, A2, B2). Scale bar: 1 μm.

about how much intensity that is bleached for both dyes, making it possible to perform a simple weighting procedure to reduce the crosstalk. The weighting procedure is similar to that of linear unmixing, previously reported for fluorescence microscopy,[27] and a detailed description can be found in the Supporting Information.

To estimate the crosstalk in real images, and to evaluate to what extent the applied intensity weighting procedure can suppress this crosstalk, we combined two images taken on separate samples of Alexa594-ab and Alexa594-phalloidin. Thereby we created a "false" dual-labeled image where we knew the exact intensity of both labels. We also combined the images taken after one bleaching-imaging step so that we could perform the procedure to extract the individual images again, as shown in Figure S7. When the original images of the separate labels were compared with the reconstructed images, the crosstalk for Alexa594-ab was estimated to ~16% into the Alexa594-phalloidin channel, and to <7% after bleaching compensation. Alexa594-phalloidin had ~18% crosstalk into Alexa594-ab channel and <6% with bleaching compensation. The crosstalk of Atto647N-ab into Dylight650-ab channel was estimated to be ~18% without compensation and <8% with bleaching compensation by the same procedure as for the Alexa594 channels. For Dylight650-ab, the bleaching procedure resulted in <1% remaining intensity. This is optimal since it will provide negligible crosstalk from Dylight650-ab to the Atto647N-ab channel. Bleaching data of the dyes can be found in the Supporting Information and is shown in Figures S5 and S6.

To summarize, the bleaching compensation, which is based on separate control samples for each target, can significantly improve the crosstalk but does not remove it completely. Two reasons for this are nonuniform bleaching in the image and photon noise. Photon noise affects the image of the bleached target since this image is reconstructed from two separate images which both have random photon noise. If bleaching compensation is performed for the stable target, it will also be affected by photon noise although to a lesser extent since the remaining intensity of the bleachable target should be low. To what extent noise affects crosstalk can be estimated by taking consecutive images of the same target and then subtracting the images from each other to see how much intensity remains, as shown in Figure S8. In our study we had ~5% crosstalk from noise for both Alexa594-ab and Atto647N-ab. The bleaching compensated crosstalk for these dyes is thus close to that coming only from noise. This type of crosstalk can be improved if a higher signal in the sample can be retrieved, since the signal-to-noise ratio scales with the square root of the number of detected photons.

Another important parameter when comparing consecutive images is the drift in the system which has to be much less than the resolution. This means that at higher resolutions the stability of the system becomes even more crucial. The drift of our system was measured to be less than 6 nm after five consecutive images and less than 8 nm after ten consecutive images acquired with the same setting (image size, pixel size and pixel dwell time) as the multicolor images. This drift is much less than our acquired resolution of 30−40 nm. See materials microscope drift for more details and Figure S9 for resolution measurement. However, if a larger drift would occur, it can be compensated by shifting the consecutive image so that the intensity profiles of the stable dye overlap with the first image.

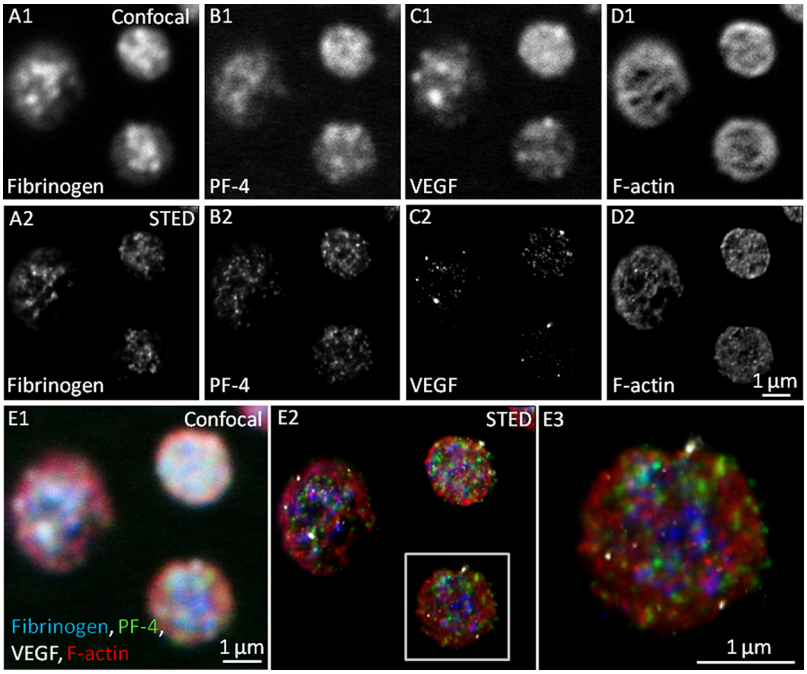

Figure 3. Four-color STED nanoscopy image. High-resolution STED images and corresponding confocal images of fibrinogen (A1, A2), PF4 (B1, B2), VEGF (C1, C2), and F-actin (D1, D2). Merged images for the confocal (E1) and STED (E2) images, as well as an enlarged STED image of a selected platelet (E3), are shown. Scale bars: 1 μm.

Four-Color STED Imaging on Platelets. Platelets contain more than 1000 different proteins.[28] The mechanisms for how platelets sequester and release specific proteins in a selective manner still remain to be clarified. We applied the described procedure for four-color STED imaging to characterize storage of proteins in platelets and to demonstrate its potential to resolve the storage mechanisms. In an earlier study we investigated how the proteins VEGF (vascular endothelial growth factor), PF-4 (platelet factor 4) and fibrinogen are stored inside the platelets in combination with filamentous actin using dual-color STED microscopy.[26] Here we perform the same type of experiment but with all four targets (VEGF, PF-4, fibrinogen, and filamentous actin) labeled in the same cells using the fluorescent dyes Alexa594-ab, Alexa594-phall, ATTO647N-ab, and Dylight650-ab (for details regarding sample preparation see Methods, Immunofluorescence Staining). This makes it possible to analyze how the individual proteins are stored in the platelets, but also to look into possible storage mechanisms and features that different proteins may have in common. A four-color STED image of the selected proteins in platelets is demonstrated in Figure 3 and Figure S11 for CMYK color scheme.

We analyzed the images by the same procedure as described in detail earlier to measure the number and size of the protein containing granules as well as their peripheral distribution.[26] The number and size were measured computationally by locating the peak intensity of the individual emission profiles and then calculating their size as the full width at half-maximum (fwhm) value. The peripheral distribution was measured using the actin image of the platelets to provide a mask of the total area spanned by the platelet. The area was then divided into five separate concentric zones of equal size (r = 1−5) where the number of proteins in each zone was measured yielding a probability distribution function, $P(r)$. The values obtained for number, size and location showed distinct features for the different proteins and agree well with earlier data, as shown in Figure 4A,B.

Since we now have all proteins labeled in the same cell, we can also add a colocalization analysis between the proteins using the Pearson correlation coefficient[29] (for more details see Methods, Image Analysis). The colocalization data showed a possible costorage of fibrinogen and PF-4 but very little overlap between VEGF and PF-4 as well as between VEGF and fibrinogen, as shown in Figure 4C. The small spatial overlap between VEGF and PF-4 is an indicator that they are stored in separate vesicles and may thus also be independently released. This corresponds well with the opposite rules of VEGF and PF-4 as pro- and antiangiogenic proteins, respectively. Taken together, by combining high resolution imaging with multiple targeting of proteins, we can now extract colocalization and spatial correlations of several targets at the same time, in the same cell, most likely offering a useful tool to elucidate how platelets orchestrate the storage and release of different regulating proteins.

Future Outlook. Since the distribution patterns of proteins are affected differently depending on the stimuli and activation of the platelet, simultaneous high resolution imaging of multiple proteins in individual platelets could provide means to separately distinguish

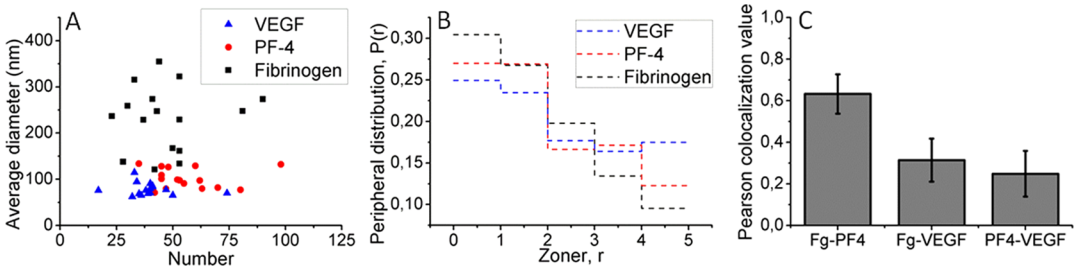

Figure 4. Analysis of platelet images. The three proteins fibrinogen, PF-4, and VEGF were analyzed in terms of number and size of the protein clusters (A), as well as their peripheral distribution (B). The colocalization of the proteins was measured by the Pearson correlation coefficient (C).

platelets based on their type of activation. Platelets are believed to play an important role in many forms of disease, where they are presumably being activated in a disease specific manner. This makes high resolution multicolor platelet imaging a possible and interesting tool for future diagnostics, as well as for elucidating the intricate regulation mechanisms for how platelets store and release proteins in a specific manner. Aside from platelet studies, high resolution imaging has been performed as a means to identify metastasizing cells based on their subcellular protein distribution patterns.[30] By increasing the number of targets, the specificity in this identification can be further increased and the amount of cells needed for a reliable diagnosis can be reduced. This could in turn provide means to use less invasive clinical diagnostic methods where the amount of extracted sample is a limitation.[31] An interesting perspective would also be to develop new analytical tools which correlate data of multiple high resolution targets. Such algorithms could give better insights into more complex cellular mechanisms, pathways and interactions where many different proteins are involved, such as in system biology elucidations.[32,33]

Regarding limitations to the technique, live-cell imaging and imaging on diffusing targets are problematic, since two or more images need to be captured where the targeted proteins should not move between captures. Also video-rate imaging will not in general be possible since only a single image can be acquired of the bleachable dye. However, if one of the targets is mainly stationary, such as motor proteins moving along a stationary fiber, the stationary target can be targeted with the bleachable dye which should allow for multitarget video-rate imaging.

For this study, we only tried few different dyes and used fixed bleaching laser wavelengths (bleaching data of the tested dyes are given in Table S1). A more thorough investigation of possible dye combinations together with fine-tuning of the bleaching wavelengths should provide better bleaching ratios and thus less crosstalk.

CONCLUSION

We successfully demonstrated four-color STED nanoscopy imaging by utilizing differences in excitation spectrum and photostability among the used fluorescent markers. The technique requires little if any changes to the optical setup and also little and very basic postprocessing. With prior knowledge regarding the bleaching of the fluorescent markers, a bleaching compensation can be added, which significantly reduces crosstalk. For our study, a crosstalk of <8% was achieved for all dyes, which is comparable or even slightly better than other multicolor nanoscopy methods.[6,7] The technique was successfully applied to image platelets where the analysis of the images is in agreement with earlier data acquired without the use of this technique. We anticipate that the combination of multicolor imaging with high resolution imaging can lead to new interesting applications such as identifying disease specific activation states of platelets and elucidating their underlying protein storage and release mechanisms. In general, it promotes the capability to exploit the spatial organization of proteins in cells for diagnostic purposes. It also opens up the development of new analytical tools and algorithms which combine information from all highly resolved color channels. Such images and algorithms could give new insights into the organization and function of multiple protein complexes where the correlative interactions of the proteins are of interest.

METHODS

Platelet Isolation and Immunofluorescence Staining. The platelets were separated from buffy coat blood sample from a healthy donor (Karolinska Hospital, Huddinge, Sweden) and prepared according to a previous protocol.[34] A detailed description of the protocol can be found in the Supporting Information.

Goat polyclonal (sc-1881) rabbit polyclonal, (sc-50301), and mouse monoclonal (sc-166968) primary antibodies (all from Santa Cruz Biotechnology, Heidelberg, Germany) were used for targeting VEGF, PF4, and fibrinogen α, respectively. Donkey polyclonal antibodies linked with Dylight650 (ab96938, Abcam, U.K.) and Alexa-594 (A12381, Life Technologies Europe BV, Sweden), as well as Phalloidin linked with Alexa-594 (A12381, Life Technologies Europe BV, Sweden), were used to stain goat and rabbit primary antibodies and actin, respectively, while sheep polyclonal was conjugated with ATTO-647N (ATTO-TEC GmbH,

Siegen, Germany) to stain mouse primary antibody. The final concentration of all the primary antibodies used for staining was ~6 μg/mL, and the final concentration for the secondary antibodies was 5 μg/mL, except for ATTO-647N conjugated sheep/anti-mouse which was chosen to be 2 μg/mL because of its higher brightness in our samples. The final concentration of Alexa-594 labeled phalloidin for actin staining was 40 nM.

The cells were fixed with 3.7% formaldehyde in DPBS for 15 min. The fixed platelets were permeabilized with Triton X-100 (0.2%) for 15 min, and then blocked for nonspecific binding with bovine serum albumin (1%, Sigma, Sweden) for 15 min. The cells were then washed once with DPBS on an orbital shaker (300 rpm), followed by incubation with primary antibodies against PF-4 (2 μg/mL), VEGF (2.5 μg/mL), or fibrinogen α (2.5 μg/mL) overnight at 4 °C. The samples were then washed twice with DPBS on an orbital shaker (300 rpm), incubated with the secondary antibody (3 μg/mL) together with Phalloidin ATTO 647N for 3 h under room temperature, and then washed three times on an orbital shaker (300 rpm) before they were mounted onto microslides with Mowiol-Dabco mounting medium (Sigma, Sweden). The detailed fixation and immunofluorescence staining protocol can be found in the literature.[26]

STED Microscopy. A custom built STED microscope was used for imaging, the principal design of which has been described in detail before.[35] The STED microscope can perform dual color imaging by having two separate excitation beams (570 ± 5 and 647 ± 5 nm), two STED beams (710 ± 10 and 750 ± 10 nm), and two emission pathways (615 ± 15 and 675 ± 15 nm). Since all wavelengths are in the orange-red spectrum, there will be little autofluorescence from the measured cells.[36] This could also be confirmed from our test experiments. The STED beams pass through separate vortex phase plates (VPP-1, RPC Photonics, Rochester, NY) imprinting helical phase masks of 2 π onto the wave-fronts. Together with circular polarization, this creates effective destructive interference at the center of the focal point and, thus, a deep central intensity minimum. Excited molecules that are outside the central minimum of the STED beam will be affected by its intensity and stimulated back to the ground state, leaving only the very central molecules to be detected. The excitation and STED beams originates from the same pulsed supercontinuum Fianium laser (SC-450-PP-HE, Fianium Ltd., Southampton, U.K.). The laser was set to 1 MHz frequency, and provides pulse duration of ~100 ps. To reduce spectral crosstalk, a time delay of 40 ns is set between the excitation and STED beams of the two respective dyes. Since the fluorescence lifetime of these dyes are just a few nanoseconds, this time separation, accompanied by the same time separation for the detectors, makes the spectral crosstalk very low (<4% Alexa594-ab and phalloidin and <3% for ATTO647N and Dylight650). The imaging powers were set to 200−500 nW for the excitation wavelengths and 0.8−1.4 mW for the STED wavelengths. The bleaching power was set to 1 mW at 710 ± 10 nm and 300 μW at 647 ± 5 nm, which is more than 2 orders of magnitude higher than the excitation power used for imaging. The image size was set to 7 × 7 μm^2 with a pixel size of 20 nm for the STED images and 50 nm for the confocal images and a pixel dwell time of 1 ms.

Drift of System. To test the drift of our system, we took several consecutive images of gold-beads, providing the reflective point spread function (PSF) of one of our STED lasers, using the same image settings (size, number of pixels, pixel dwell time) as for the platelet imaging as shown in Figure S10. The center positions of the gold beads were then computationally calculated for each image by fitting the images with the STED PSF using convolution. The bead positions were determined as the pixels providing the highest fitting values and the location of these pixels were measured, stored and then compared for each consecutive image.

Fluorometer. Excitation spectra of the dyes were recorded from ~1 μM concentrated dye solution in cuvettes by a spectrofluorometer (FluoroMax-3, Horiba Jobin-Yvon, Edison, NJ).

Image Processing. Images were acquired using the software Imspector (Department of NanoBiophotonics, MPI for Biophysical Chemistry, Göttingen, Germany) providing raw data images where each pixel value corresponds to the measured number of emitted photons in that pixel. To preserve the raw data, images were exported as .dat files and then imported and processed in Matlab (MathWorks, Inc., Natick, MA). Image subtraction was performed by taking the raw data of one image and subtracting it from the raw data of another image with or without weighting. The platelet images were deconvoluted using 10 iterations of the Richardsson-Lucy deconvolution algorithm using a 40 nm Lorentzian point spread function (PSF) before analysis.[37]

Image Analysis. The analysis of the platelet images have been described in detail before regarding number, size and distribution.[26] For colocalization, the Pearson correlation coefficient was used:[38]

$$P = \frac{\sum_{i=1}^{n} (G_i - \bar{G})(R_i - \bar{R})}{\sum_{i=1}^{n} \sqrt{(G_i - \bar{G})^2} \sum_{i=1}^{n} \sqrt{(R_i - \bar{R})^2}}$$

where G_i and R_i are the intensity values at pixel i for images G and R, respectively, and n is the total amount of pixels.

Statistics. Four consecutive images were taken on at least five separate cells for both imaging and bleaching data of the studied fluorescent molecules. Three separate measurements were performed to test the crosstalk with and without bleaching compensation for each dye. Data from 16 cells from a single blood donor were used for analyzing the number, size, distribution and colocalization of the studied proteins.

Conflict of Interest: The authors declare no competing financial interest.

Acknowledgment. This work was supported by Cancerfonden (CAN 2011/654) and the European 7th framework program (FLUODIAMON, 801237). We thank Hans Blom (SciLifeLab-Stockholm) for fruitful discussions regarding the technique and support in establishing the microscope, Zhangsen Huang and Linjing Zhu (Karolinska Institute-Stockholm) for sharing their expertise in how to treat and handle platelets, and finally Stefan W. Hell, Lars Kastrup, and Andreas Schönle (MPIBPC-Göttingen) for support in establishing the microscope and for the Imspector software.

Supporting Information Available: Details regarding the weighting compensation for crosstalk reduction and platelet sample preparation, as well as images showing excitation spectrum of dyes, cytoskeletal images, crosstalk schematics, bleaching of dyes, crosstalk compensation, noise effects and microscope resolution. This material is available free of charge *via* the Internet at http://pubs.acs.org.

REFERENCES AND NOTES

1. Carlsson, K.; Danielsson, P. E.; Lenz, R.; Liljeborg, A.; Majlöf, L.; Åslund, N. Three-Dimensional Microscopy using a Confocal Laser Scanning Microscope. *Opt. Lett.* **1985**, *10*, 53–55.
2. Hell, S. W.; Wichmann, J. Breaking the Diffraction Resolution Limit by Stimulated Emission: Stimulated-Emission-Depletion Fluorescence Microscopy. *Opt. Lett.* **1994**, *19*, 780–782.
3. Klar, T. A.; Hell, S. W. Subdiffraction Resolution in Far-Field Fluorescence Microscopy. *Opt. Lett.* **1999**, *24*, 954–956.
4. Betzig, E.; Patterson, G. H.; Sougrat, R.; Lindwasser, O. W.; Olenych, S.; Bonifacino, J. S.; Davidson, M. W.; Lippincott-Schwartz, J.; Hess, H. F. Imaging Intracellular Fluorescent Proteins at Nanometer Resolution. *Science* **2006**, *313*, 1642–1645.
5. Rust, M. J.; Bates, M.; Zhuang, X. W. Sub-Diffraction-Limit Imaging by Stochastic Optical Reconstruction Microscopy (STORM). *Nat. Methods* **2006**, *3*, 793–795.
6. Dempsey, G. T.; Vaughan, J. C.; Chen, K. H.; Bates, M.; Zhuang, X. Evaluation of Fluorophores for Optimal Performance in Localization-Based Super-Resolution Imaging. *Nat. Methods* **2011**, *8*, 1027–1036.
7. Bückers, J.; Wildanger, D.; Vicidomini, G.; Kastrup, L.; Hell, S. W. Simultaneous Multi-Lifetime Multi-Color STED Imaging for Colocalization Analyses. *Opt. Express* **2011**, *19*, 3130–3143.

8. Hell, S. W. Far-Field Optical Nanoscopy. *Science* **2007**, *25*, 1153–1158.
9. Hell, S. W. Microscopy and its Focal Switch. *Nat. Methods* **2009**, *6*, 24–32.
10. Thompson, R. E.; Larson, D. R.; Webb, W. W. Precise Nanometer Localization Analysis for Individual Fluorescent Probes. *Biophys. J.* **2002**, *82*, 2775–2783.
11. Bates, M.; Dempsey, G. T.; Chen, K. H.; Zhuang, X. Multicolor Super-Resolution Fluorescence Imaging *via* Multi-Parameter Fluorophore Detection. *ChemPhysChem.* **2012**, *16*, 99–107.
12. Chang, C.; Sud, D.; Mycek, M. Fluorescence Lifetime Imaging Microscopy. *Methods Cell Biol.* **2007**, *81*, 495–524.
13. Whiteheart, S. W. Platelet Granules: Surprise Packages. *Blood* **2011**, *118*, 1370.
14. Chatterjee, M.; Huang, Z.; Zhang, W.; Jiang, L.; Hultenby, K.; Zhu, L.; Hu, H.; Nilsson, G. P.; Li, N. Distinct Platelet Packaging, Release, and Surface Expression of Proangiogenic and Antiangiogenic Factors on Different Platelet Stimuli. *Blood* **2011**, *117*, 3907–3911.
15. Tjoelker, L. W.; Stafforini, D. M. Platelet-Activating Factor Acetylhydrolases in Health and Disease. *Biochim. Biophys. Acta* **2000**, *1488*, 102–123.
16. Peplow, P. V. Regulation of Platelet-Activating Factor (PAF) Activity in Human Diseases by Phospholipase A2inhibitors, PAF Acetylhydrolases, PAF Receptor Antagonists and Free Radical Scavengers. *Prostaglandins, Leukotrienes Essent. Fatty Acids* **1999**, *61*, 65–82.
17. Farndale, R. W. Collagen-Induced Platelet Activation. *Blood Cells, Mol., Dis.* **2006**, *36*, 162–165.
18. Okamura, Y.; Schmidt, R.; Raschke, I.; Hintze, M.; Takeoka, S.; Egner, A.; Lang, T. A Few Immobilized Thrombins are Sufficient for Platelet Spreading. *Biophys. J.* **2011**, *100*, 1855–1863.
19. Wolberg, A. S. Thrombin Generation and Fibrin Clot Structure. *Blood Rev.* **2007**, *21*, 131–142.
20. Battinelli, E. M.; Markens, B. A.; Italiano, J. E. J. Release of Angiogenesis Regulatory Proteins from Platelet Alpha Granules: Modulation of Physiologic and Pathologic Angiogenesis. *Blood* **2011**, *118*, 1359–1369.
21. Coller, B. S. Historical Perspective and Future Directions in Platelet Research. *J. Thromb. Haemostasis* **2011**, *9*, 374–395.
22. Feng, W.; Madajka, M.; Kerr, B. A.; Mahabeleshwar, G. H.; Whiteheart, S. W.; Byzova, T. V. A Novel Role for Platelet Secretion in Angiogenesis: Mediating Bone Marrow-Derived Cell Mobilization and Homing. *Blood* **2011**, *117*, 3893–3902.
23. Italiano, J. E. J.; Richardson, J. L.; Patel-Hett, S.; Battinelli, E.; Zaslavsky, A.; Short, S.; Ryeom, S.; Folkman, J.; Klement, G. L. Angiogenesis is Regulated by a Novel Mechanism: Pro- and Antiangiogenic Proteins are Organized into Separate Platelet α Granules and Differentially Released. *Blood* **2008**, *111*, 1227–1233.
24. Kamykowski, J.; Carlton, P.; Sehgal, S.; Storrie, B. Quantitative Immunofluorescence Mapping Reveals Little Functional Coclustering of Proteins within Platelet α-granules. *Blood* **2011**, *118*, 1370–1373.
25. van Nispen tot Pannerden, H.; de Haas, F.; Geerts, W.; Posthuma, G.; van Dijk, S.; Heijnen, H. F. G. The Platelet Interior Revisited: Electron Tomography Reveals Tubular α-granule Subtypes. *Blood* **2010**, *116*, 1147–1156.
26. Rönnlund, D.; Yang, Y.; Blom, H.; Auer, G.; Widengren, J. Fluorescence Nanoscopy of Platelets Resolves Platelet-State Specific Storage, Release and Uptake of Proteins, Opening for Future Diagnostic Applications. *Adv. Healthcare Mater.* **2012**, *1*, 707–713.
27. Zimmermann, T.; Marrison, J.; Hogg, K.; O'Toole, P. Clearing Up the Signal: Spectral Imaging and Linear Unmixing in Fluorescence Microscopy. *Methods Mol. Biol.* **2014**, *1075*, 129–148.
28. Michelson, A. D. The Platelet Proteome. In *Platelets*; Academic Press: Amsterdam, 2012; p 103.
29. Adler, J.; Parmryd, I. Quantifying Colocalization by Correlation: The Pearson Correlation Coefficient is Superior to the Mander's Overlap Coefficient. *Cytometry, Part A* **2010**, *77A*, 733–742.
30. Rönnlund, D.; Gad, A. K. B.; Blom, H.; Aspenström, P.; Widengren, J. Spatial Organization of Proteins in Metastasizing Cells. *Cytometry, Part A* **2013**, *83*, 855–865.
31. Wiksell, H.; Ekstrand, V.; Wadström, C.; Auer, G. A New Specially Designed Needle Significantly Increases Sample Yield during Fine Needle Aspiration of Breast Lesions. *Phys. Med.* **2009**, *25*, 47–50.
32. Lubeck, E.; Cai, L. Single-Cell Systems Biology by Super-Resolution Imaging and Combinatorial Labeling. *Nat. Methods* **2012**, *9*, 743–748.
33. Barabási, A.-L.; Oltvai, Z. N. Network Biology: Understanding the Cell's Functional Organization. *Nat. Rev. Genet.* **2004**, *5*, 101–113.
34. Jiang, L.; Song, X. H.; Liu, P.; Zeng, C. L.; Huang, Z. S.; Zhu, L. J.; Jiang, Y. Z.; Ouyang, H. W.; Hu, H. Platelet-Mediated Mesenchymal Stem Cells Homing to the Lung Reduces Monocrotaline-Induced Rat Pulmonary Hypertension. *Cell Transplant.* **2012**, *21*, 1463–1475.
35. Wildanger, D.; Rittweger, E.; Kastrup, L.; Hell, S. W. STED Microscopy with a Supercontinuum Laser. *Opt. Express* **2008**, *16*, 9614–9621.
36. Monici, M. Cell and Tissue Autofluorescence Research and Diagnostic Applications. *Biotechnol. Annu. Rev.* **2005**, *11*, 227–256.
37. Richardson, W. H. Bayesian-Based Iterative Method of Image Restoration. *J. Opt. Soc. Am.* **1972**, *62*, 55–59.
38. Manders, E. M.; Stap, J.; Brakenhoff, G. J.; Driel, R. v.; Aten, J. A. Dynamics of Three-Dimensional Replication Patterns during the S-phase, Analysed by Double Labelling of DNA and Confocal Microscopy. *J. Cell Sci.* **1992**, *103*, 857–862.